Thin Solid Films 659 (2018) 24–35

Contents lists available at ScienceDirect

Thin Solid Films

journal homepage: www.elsevier.com/locate/tsf

Nucleation and growth of oriented metal-organic framework thin films on thermal SiO_2 surface

Ki-Joong Kim[a,1], Yujing Zhang[a], Peter B. Kreider[a], Xinyuan Chong[b], Alan X. Wang[b], Paul R. Ohodnicki Jr[c], John P. Baltrus[c], Chih-Hung Chang[a,*]

[a] School of Chemical, Biological & Environmental Engineering, Oregon State University, Corvallis, OR 97331, United States
[b] School of Electrical Engineering & Computer Science, Oregon State University, Corvallis, OR 97331, United States
[c] National Energy Technology Laboratory (NETL), U.S. Department of Energy, 626 Cochrans Mill Road, Pittsburgh, PA 15236, United States

ARTICLE INFO

Keywords:
Metal-organic framework
Thin film
Layer-by-layer deposition
Oriented growth
Copper benzene-1,3,5-tricarboxylate
X-ray photoelectron spectroscopy

ABSTRACT

Assembly of metal-organic framework (MOF) thin-films with well-ordered growth directions enables many practical applications and is likely part of the future of functional nanomaterials. Insights into the formation pathway of the MOF thin films would allow better control over the growth directions and possibly the amount of guest molecules absorbed into the MOF pores. Here, we investigate the nucleation and growth of oriented $Cu_3(BTC)_2{\cdot}xH_2O$ MOF (HKUST-1, BTC = benzene-1,3,5-tricarboxylic acid) thin films on the thermal SiO_2 surface using a room temperature stepwise layer-by-layer (LBL) method. Initial stages of LBL growth were characterized with X-ray photoelectron spectroscopy and high-resolution transmission electron microscopy analysis in order to understand nucleation and growth kinetics. HKUST-1 thin films with preferred growth along the [111] direction on the thermal SiO_2 surface were obtained in the absence of not only a gold substrate, but also organic-based self-assembled monolayers (SAMs). It is found that the formation of HKUST-1 is initiated by deposition of copper acetate on the thermal SiO_2 surface followed by ligand exchange between coordinated acetate from the copper precursor and the BTC ligands. As the LBL growth cycle is increased, HKUST-1 crystals on the thermal SiO_2 surfaces are continuously forming and growing and finally the crystallites coalesce into a continuous film. Highly oriented HKUST-1 thin films on thermal SiO_2 surface with complete surface coverage and ~90 nm thickness were obtained at ~80 cycles of LBL growth under the conditions used in this study.

1. Introduction

Nanoporous metal-organic framework (MOF)-based thin films have become an increasingly popular research topic in nanotechnological fields, particularly for applications in luminescence, chemical sensing, catalysis, membranes and optical devices [1–5]. A clear understanding of nucleation and growth of MOF-based thin film is important to control the resulting film's structure and its properties [6].

There are several approaches that have been reported for preparation of MOF thin films: (1) direct growth from solvothermal mother solutions, (2) assembly of preformed nanocrystals, (3) layer-by-layer (LBL) stepwise growth, (4) electrochemical deposition of MOF thin films on conductive substrates, and (5) deposition of MOF thin films by a gel-layer approach. The room temperature stepwise LBL approach yields uniform, high-quality MOF thin films and can be repeated to create targeted thicknesses, allowing for the additional advantages of fine-tuned thickness control and the ability to create multilayer MOF thin films [7–12]. Currently, gold substrates functionalized by thiol-based self-assembled monolayers (SAMs) [7–24], such as 16-mercaptohexadecanoic acid, 11-mercaptoundecanoic acid, 11-mercaptoundecanol, and 4,(4-pyridyl)phenyl-methanethiol, are used to facilitate preferential nucleation of MOFs and subsequent oriented film growth. However, the use of these SAMs could pose some limitations due to their thermal and chemical instability [25]. Another potential issue with thiol-based SAMs is their insulating nature, which could result in poor electrical contact. Therefore, a capability to grow oriented MOF thin films in the absence of thiol-based organic SAMs could resolve these potential issues. Herein, we present such a concept based on a

* Corresponding author.
E-mail address: chih-hung.chang@oregonstate.edu (C.-H. Chang).
[1] Current address: National Energy Technology Laboratory (NETL), U.S. Department of Energy, 626 Cochrans Mill Road, Pittsburgh, PA 15236, United States.

https://doi.org/10.1016/j.tsf.2018.05.026
Received 10 November 2017; Received in revised form 8 May 2018; Accepted 10 May 2018
Available online 16 May 2018

$Cu_3(BTC)_2{\cdot}xH_2O$ MOF (HKUST-1, BTC = benzene-1,3,5-tricarboxylic acid) supported on oxide substrates such as a thermal SiO_2 surface on a silicon wafer, which is important for the fabrication of many functional devices such as chemical sensors. Several methods such as an O_2 plasma and other chemical treatments have been used to effectively create OH− on the oxide surface in order to promote uniform MOF film nucleation and growth, but the density of films synthesized in this way varies and is difficult to control. For example, the growth of MOF thin films on metal oxide surfaces (SiO_2 and Al_2O_3) treated by an O_2 plasma has been examined [22], however the resulting MOF films show only a slightly preferred orientation. Therefore, it is important to understand the nucleation and growth kinetics of MOFs using a stepwise LBL method in order to obtain uniform, dense and highly-oriented thin films.

In this study, we elucidated the growth pathway for the formation of highly oriented MOF thin films. As part of this strategy, thermal SiO_2 layers were used because high quality nonstoichiometric SiO_x ($x < 2$) layers can be simply generated by thermal oxidation of a silicon wafer in air and the material is technologically important in many optoelectronics. HKUST-1 was chosen as a model compound because it is the most widely studied MOF material in thin-film applications and has good performance for gas storage and separations [4,26,27].

2. Experimental

2.1. Materials

Copper acetate ($Cu(OAc)_2$, 98%) and benzene-1,3,5-tricarboxylic acid (BTC, 95%) were purchased from Sigma-Aldrich. Copper nitrate hexahydrate ($Cu(NO_3)_2{\cdot}6H_2O$, 98%) was obtained from Alfa Aesar. ACS grade ethanol (> 99.5%) from Macron chemicals was used as the solvent. All chemicals were used as purchased without further purification. N-type one-side polished silicon wafer from SUMCO was used for the substrate. Quartz, glass, and sapphire substrates were purchased from SPI Supplies.

2.2. Preparation of HKUST-1 thin films

Substrates were cleaned via sonication in a three step process: (1) 15 min in deionized water; (2) 15 min in acetone; (3) 15 min in isopropanol. Three rinses were performed between each sonication step. Then the substrates were treated by O_2 plasma at 20 W for 10 min. A thin layer of thermal SiO_2 on the surface of the silicon wafer was grown by thermal oxidation at 1000 °C in air. Different thermal SiO_2 layers were obtained by changing the thermal oxidation times. A room temperature stepwise LBL method was used to grow the HKUST-1 thin films on the thermal SiO_2 surface.

The substrates were immersed in 30 mL of 1 mmol ethanol solution of the metal precursor ($Cu(OAc)_2$) for 20 min. Subsequently, the substrate was immersed in 30 mL of 0.1 mmol ethanol solution of the organic ligand (BTC) for 40 min. Between each step, the substrates were rinsed with ethanol to remove unreacted precursor ions or molecules and to ensure uniform film growth and then dried in a N_2 stream.

Powder-type bulk HKUST-1 was synthesized by a solvothermal method in a continuous flow microreactor-assisted system reported in our previous work [28]. The collected reaction products were washed with ethanol 3 times and dried under vacuum for 24 h at 70 °C for further characterization.

2.3. Characterization

X-ray diffraction (XRD) patterns were obtained using a Rigaku Ultima IV Diffractometer, operating at 40 kV and 40 mA with Cu kα radiation (0.154 nm) in the range from 5 to 20° with a step size of 0.01. Field emission-scanning electron microscope (FE-SEM) analysis was conducted with an FEI Quanta 600 and FEI Nova NanoSEM 230 using 5–10 kV accelerating voltage. Atomic force microscopy (AFM) images were obtained using a Bruker Innova microscope in tapping mode with a Si cantilever. Attenuated total reflectance (ATR) infrared spectra were collected with a Thermo Scientific Nicolet 6700 Fourier transform infrared (FT-IR) spectrometer and Thermo Scientific Smart

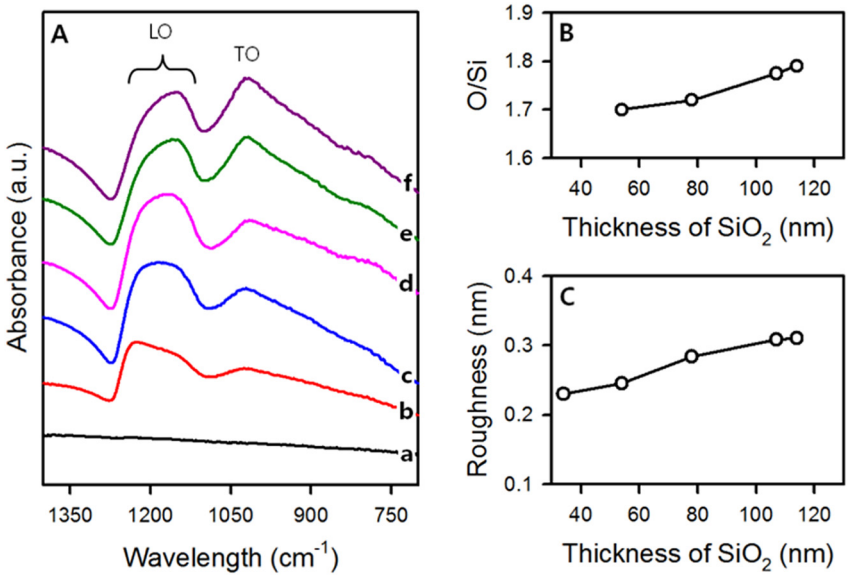

Fig. 1. (A) ATR infrared spectra (a: bare Si, b: 34 nm-SiO_2, c: 54 nm-SiO_2, d: 78 nm-SiO_2, e: 107 nm-SiO_2, and f: 114 nm-SiO_2), (B) atomic oxygen to silicon ratio, O/Si, obtained from XPS, and (C) surface roughness confirmed by AFM of the thermal SiO_2 surface with different thickness of SiO_2 layers.

iTR diamond ATR accessory. The contact angle was measured using a FTA135 Contact Angle Analyzer with a 1 μL deionized water droplet. High resolution transmission electron microscopy (HRTEM) images and atomic resolution high-angle annular dark-field scanning TEM (HAADF-STEM) images were obtained using an FEI Titan 80–300 operating at 300 kV. A commercial TEM grid from Ted Pella with a 40 nm thick thermal SiO_2 layer was used. Average particle sizes were determined by manually counting at least 100 particles in the micrographs. X-ray photoelectron spectroscopy (XPS) was carried out with a PHI 5600ci instrument using a monochromatized Al Kα X-ray source (1486.6 eV). The pass energy of the analyzer was 23.5 eV. Binding energies were calibrated using the C 1 s signal for adventitious carbon, which was assigned a binding energy of 285.0 eV [29]. Atomic ratios were calculated based on sensitivity factors provided by the instrument manufacturer. Curve fitting of the C 1 s spectra was done using CasaXPS software.

3. Results and discussion

First, characteristics of the thermal SiO_2 layer with different SiO_2 thicknesses and their relationship with the MOF growth were investigated in detail using FT-IR, XPS, AFM, and contact angle measurements. Fig. 1 shows ATR infrared spectra, XPS-derived atomic oxygen to silicon ratios, O/Si, and surface roughness of the thermal SiO_2 surface with different SiO_2 layer thicknesses. ATR infrared spectra of the thermal SiO_2 surface show two absorption bands at

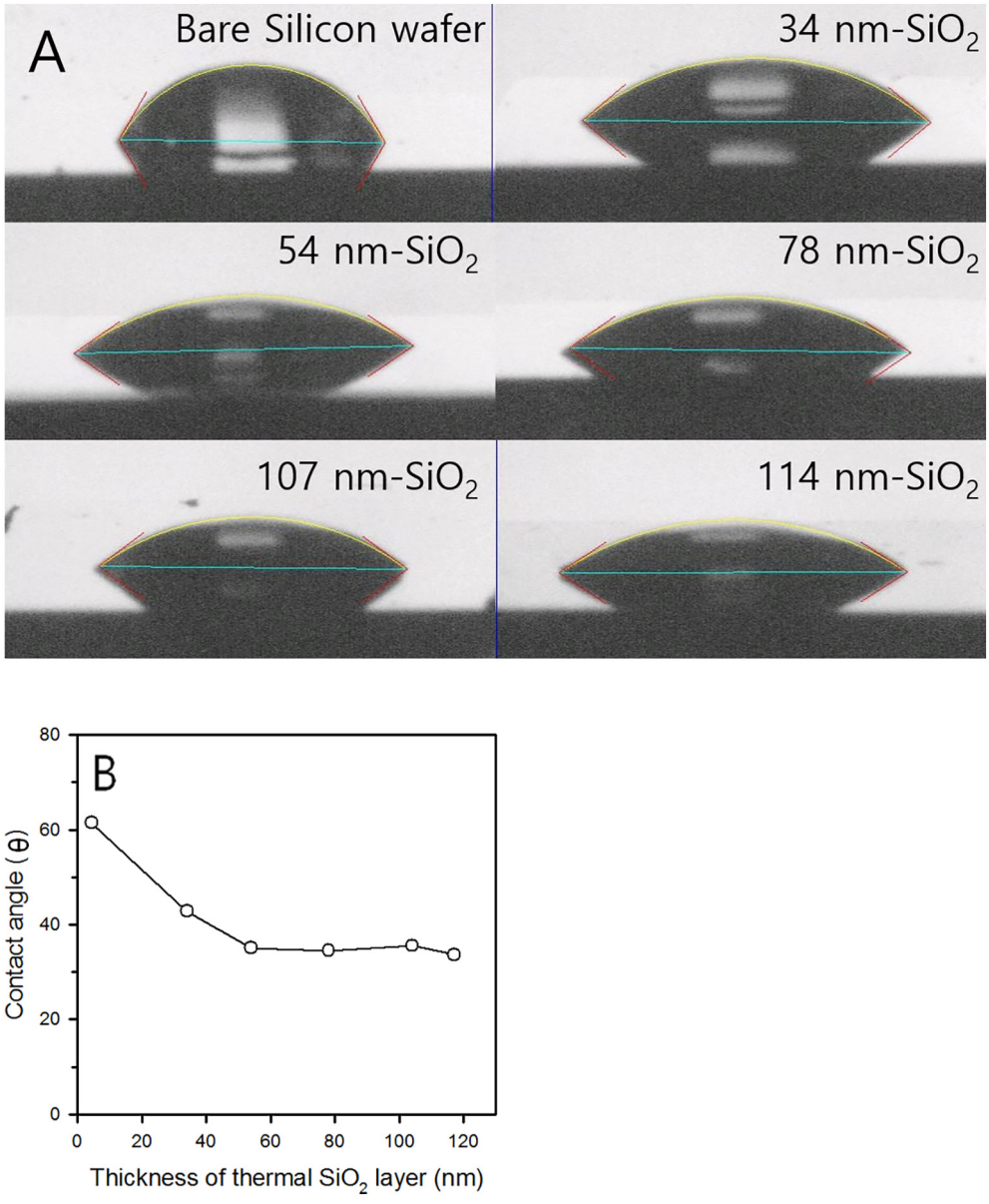

Fig. 2. (A) Photo-images and (B) water contact angle measurements of the bare silicon wafer and thermal SiO_2 surface with different thermal SiO_2 layers.

around 1150–1250 cm^{-1} and at 1020 cm^{-1} which correspond to the longitudinal optical (LO) band and the transverse optical (TO) band of the Si-O-Si stretching mode, respectively (Fig. 1A) [30,31]. The relative intensity of the TO band increases when the thickness of the thermal SiO_2 layer increases. This proves that the silicon atoms bond with increasing amounts of oxygen atoms in the lattice structure during the thermal oxidation process, leading to increasing oxygen content in the nonstoichiometric SiO_x produced as the thickness of the oxide layer increases (Fig. 1B) [32]. We also observed a shift in the position of the LO mode band with increasing oxygen content in the SiO_2 layer. Surface roughness increased with slightly increasing thermal SiO_2 thickness, confirmed by AFM (Fig. 1C). Note that there is no direct evidence of OH− on the surface of thermal SiO_2 surface from ATR infrared results.

As the thickness of SiO_2 increases, the hydrophilicity of the surface increases as a result of the increase in the amount of $Si(-O)_2$, and any OH− groups formed on the surface. An increase in oxide thickness beyond 54 nm (up to 114 nm) did not result in a significant change in the hydrophilicity of the thermal SiO_2 surface (Fig. 2).

Next, we investigated MOF growth on bare silicon and thermal SiO_2 surfaces. As revealed by SEM images, particle growth is sparse on the bare silicon surface (Fig. 3A). In contrast, more dense particles are formed after 20 cycles of LBL growth on the thermal SiO_2 surface as shown in the SEM images (Figs. 3B-3F), indicating strong interaction between the thermal SiO_2 surface and precursors. HKUST-1 growth on the thermal SiO_2 surface with different SiO_2 thicknesses was examined because we expected that differences in substrate wettability and surface roughness would affect HKUST-1 deposition. Similar surface coverages were found after 20 cycles of LBL growth on different thermal SiO_2 thicknesses. However, AFM data (Fig. 4) shows a small increase in surface roughness of the HKUST-1 films with increasing thickness of the thermal SiO_2 layer. The rougher films presumably have higher surface areas, which might lead to enhanced growth rate by LBL cycling. This is supported by the XRD results showing a small increase in XRD peak intensities (Fig. 5). In addition, the growth of a HKUST-1 thin film after 20 cycles LBL growth was highly oriented along the [111] direction on thermal SiO_2 surfaces.

It was found that a HKUST-1 film at 20 cycles LBL growth shows locally nucleated crystals on the thermal SiO_2 surface as opposed to uniform and continuous film growth. Therefore, further investigations at initial LBL growth have been carried out in order to explore the interactions between the thermal SiO_2 surface and chemical species in the precursor solution. XPS analysis was performed on three different substrates: bare thermal SiO_2, thermal SiO_2 immersed in $Cu(OAc)_2$ solution, and thermal SiO_2 immersed in BTC solution. In the C 1 s spectrum (Fig. 6A) two significant peak envelopes are identified for the first step immersion into $Cu(OAc)_2$ solution. One is at 285.0 eV and is assigned primarily to adventitious carbon and carbon bonded to hydrogen, while a smaller peak at 289.0 eV is attributed to the carboxylate group (O═C−O) in $Cu(OAc)_2$ [33,34]. This result indicates that nucleation starts immediately after immersion into the $Cu(OAc)_2$ solution. A peak at ~289.0 eV corresponding to the three carbon atoms of the carboxyl groups in BTC [35] does not appear after immersion into H_3BTC solution, indicating that there are no direct interactions between BTC and the thermally produced SiO_2 surface. Note that there is no difference in binding energies between the carbon atoms of the carboxylate group in $Cu(OAc)_2$ and the carboxyl group in BTC.

The XPS spectrum of the Cu $2p_{3/2}$ region following the first step immersion in $Cu(OAc)_2$ solution revealed peaks, which can be correlated to Cu^+ (933.8 eV) and Cu^{2+} (935.4, 941.8 and 944.6 eV) states, respectively (Fig. 6B). The two higher binding energy peaks are from the shake-up satellite features associated with the Cu^{2+} on the thermal SiO_2 surface [36,37]. It should be noted that the source of the Cu^+ state was confirmed to be a result of XPS-induced reduction of Cu^{2+} [36]. The Cu $2p_{3/2}$ binding energies are higher than what are reported for the corresponding bulk oxides for these two oxidation states of Cu (Cu^{2+}). This behavior has been reported many times for Cu-containing species on oxide supports, especially those supported on SiO_2, and has been attributed to various phenomenon including the nature of the interactions between the supported moieties and the support [38,39]. The high value for the Cu 2p binding energy measured here is typically associated with low Cu concentrations well-dispersed on the support, which is what would be expected after a single immersion in the $Cu(OAc)_2$ solution [38,39]. The XPS analysis combined with the results of the other characterization techniques supports that stepwise LBL growth of HKUST-1 on the thermal SiO_2 surface is initiated by deposition of $Cu(OAc)_2$ on the surface, followed by ligand exchange between coordinated acetate from the copper precursor and BTC ligands, leading to crystallite coalescence to form a dense film.

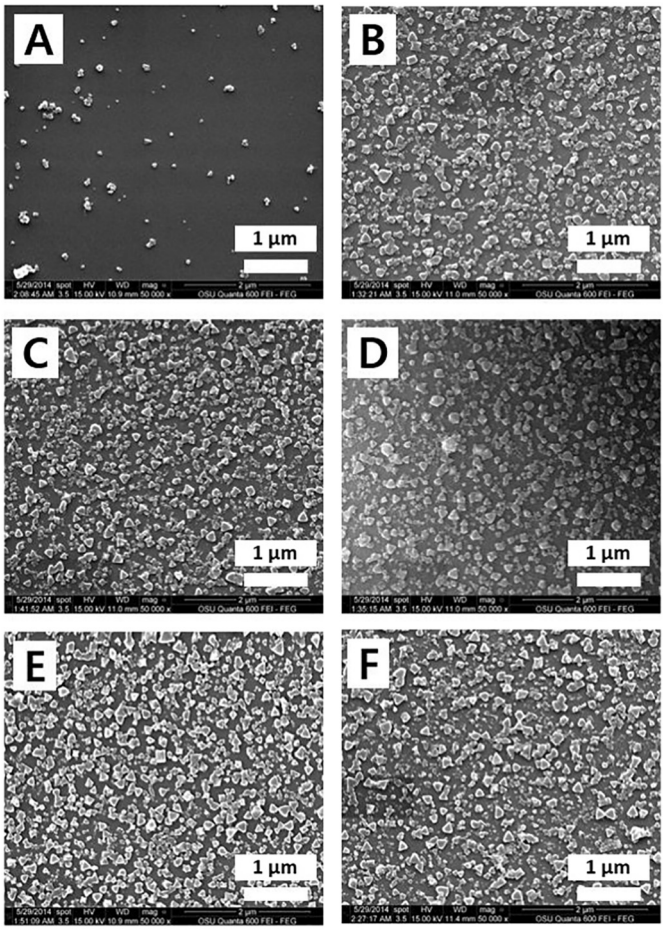

Fig. 3. FE-SEM images of the HKUST-1 thin films after 20 cycles LBL growth (A) on bare silicon wafer, (B) on 34 nm SiO_2 layer, (C) on 54 nm SiO_2 layer, (D) on 78 nm SiO_2 layer, (E) on 107 nm SiO_2 layer, and (F) on 114 nm SiO_2 layer.

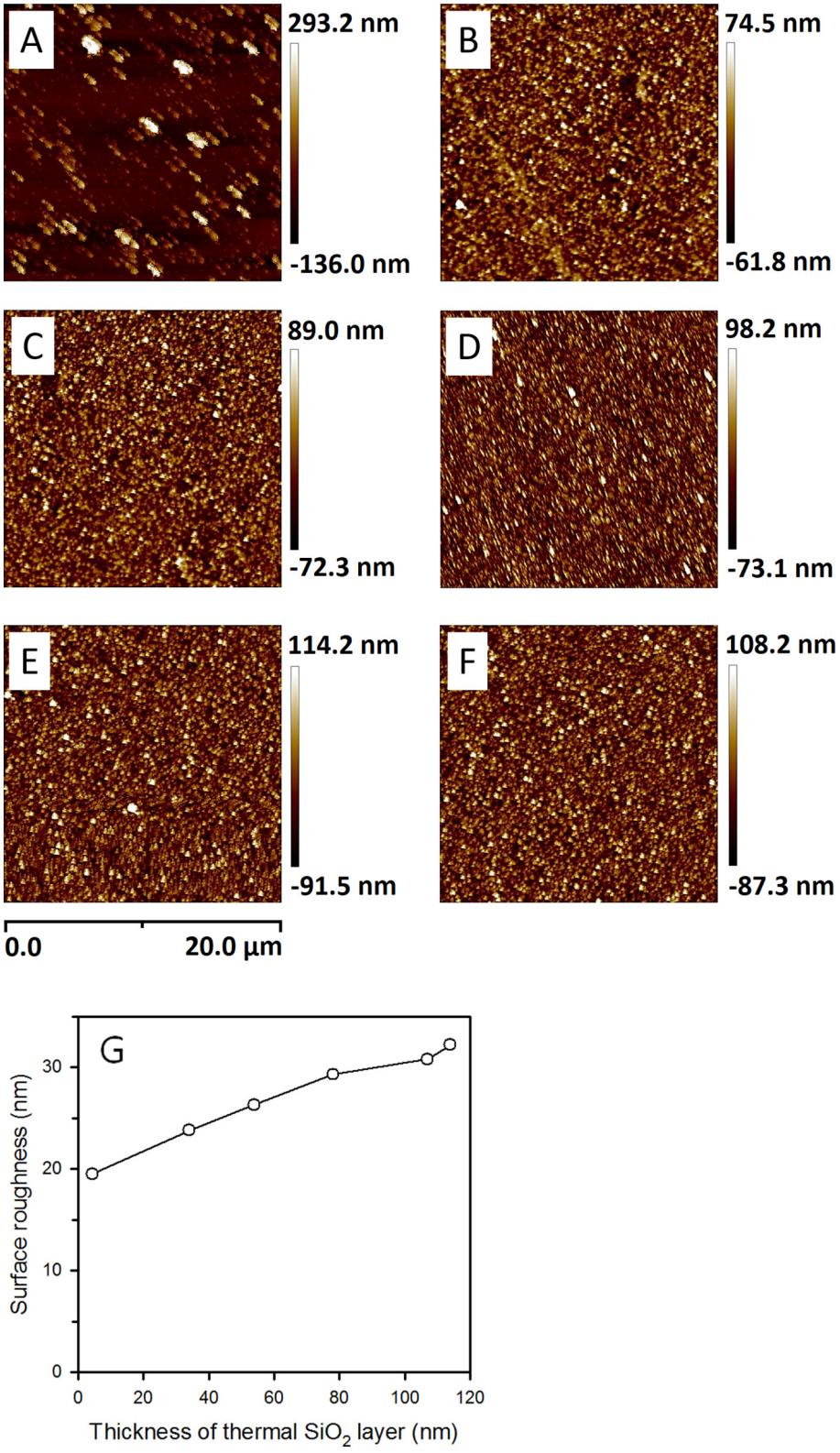

Fig. 4. AFM images of the HKUST-1 thin films after 20 cycles LBL growth (A) on bare silicon wafer, (B) on 34 nm SiO_2 layer, (C) on 54 nm SiO_2 layer, (D) on 78 nm SiO_2 layer, (E) on 107 nm SiO_2 layer, and (F) on 114 nm SiO_2 layer. (G) Surface roughness confirmed by AFM of HKUST-1 films versus thickness of thermal SiO_2 layer.

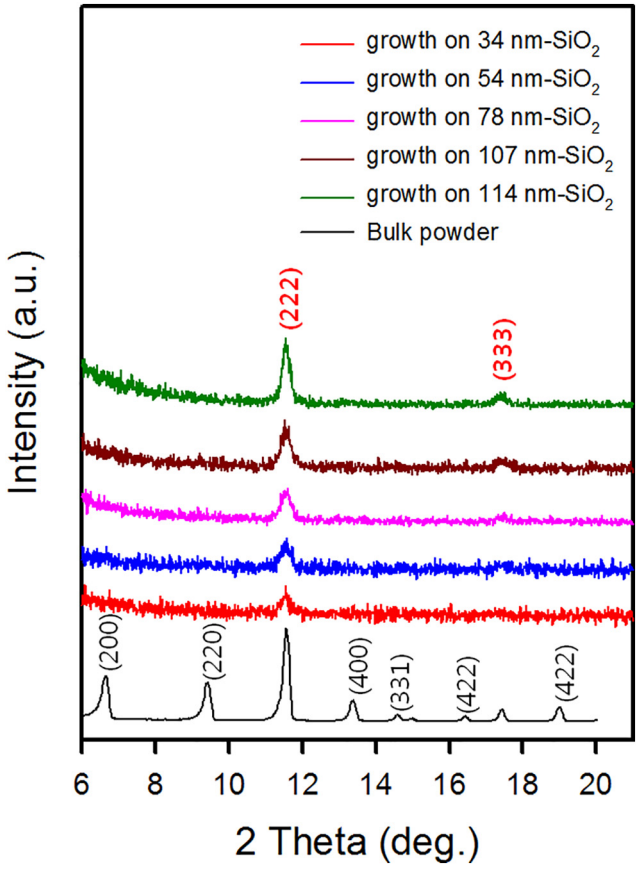

Fig. 5. XRD patterns of the HKUST-1 thin films after 20 cycles LBL method growth on thermal SiO_2 surface with different thermal SiO_2 layers.

In the FT-IR spectra (Fig. 6C), the band observed around 1715 cm^{-1} can be assigned to the H-bonded C═O stretching vibration in BTC [40], which is shifted to 1655 cm^{-1} after complexation with Cu^{2+}, suggesting that deprotonation has occurred. This indicates that the carboxylate groups (RCOO-) of BTC are coordinated to Cu^{2+} during nucleation of the HKUST-1 crystal structure.

Nucleation and growth kinetics of HKUST-1 on a thermal SiO_2 surface were also investigated by HRTEM analysis, with special attention given to samples at low LBL cycles. A commercial TEM grid with a thermally grown 40 nm SiO_2 layer was used as the growth substrate. Representative TEM (or STEM) and SEM images of the grown HKUST-1 are shown in Fig. 7. It can be seen that very small particles with an average size of 2.7 nm are formed at 2 cycles LBL growth (Fig. 7A). At 4 cycles and 6 cycles LBL growth, larger particles were observed with an average size of 4.5 nm (Fig. 7B) and 8.3 nm (Fig. 7C), respectively (See the average particle sizes at each LBL cycle in Fig. 8). HRTEM imaging (insert of Fig. 7C) reveals single crystals and aligned pores with a lattice distance of 0.35 nm, illustrative of the tetrahedron-shaped side pockets viewed along the [111] direction associated with HKUST-1. The inset in Fig. 7C also shows the crystallographic structure from the [111] direction with triangular windows. It is interesting that the different morphologies showing a hexagonal shaped unit cell viewed along the [111] direction [41] are observed for 8 cycles of LBL growth with an average size of about 25.2 nm (Fig. 7D and E). After 10 cycles of LBL growth (Fig. 7F), a significant increase to an average size of 92.7 nm with clear triangular shaped single crystals can be observed on the thermal SiO_2 surface. The morphology of the crystals matches well with the typical [111] facets of HKUST-1 reported in the literature [42–44]. Concomitant with this crystal size increase is a fairly wide particle size distribution for 10 cycles of LBL growth (Fig. 8).

We therefore propose that the LBL growth starts with formation of small single nanoparticles on thermal SiO_2 surfaces, which then join together as their density becomes greater and form the inter-grown larger crystallites with increasing LBL cycles. This is expected to result in a significant increase in average particle size when the particle coalescence rate is greater than the nucleation rate on the thermal SiO_2 surface. Triangular shapes with [111] facets that can grow on the thermal SiO_2 surface are clearly observed as the number of LBL cycles is increased (Fig. 7G). Thus the [111] direction appears to be favored for selective crystal growth on a thermal SiO_2 surface, eventually resulting in complete coverage by a thin film.

To further investigate the growth kinetics of HKUST-1 at high LBL cycles on the thermal SiO_2 surface with a 107 nm-SiO_2 layer, a correlation between the HKUST-1 film thickness and number of LBL growth cycles was performed. SEM images show that the surface coverage of the HKUST-1 thin films proportionally increases when the number of LBL cycles increases (Figs. 9A-9E). The LBL synthesis led to a stepwise growth of HKUST-1 on the thermal SiO_2 surface and the film thickness increases at a rate of 1.143 nm per cycle (Fig. 9F). This value is in very good agreement with the deposition of a secondary building unit with step heights of 1.1 nm to 1.5 nm per cycle at the [111] surface of HKUST-1 [45,46]. This result indicates an ideal LBL growth of HKUST-1 films under the conditions used in this study. Cross-sectional SEM images at different number of cycles show that homogeneous HKUST-1 thin films can be obtained by increasing the number of LBL growth cycles. Uniform thin films with complete surface coverage were observed after 80 cycles of LBL growth and the thickness of this film was about 87.5 ± 9.4 nm. The surface roughness was observed to decrease as the film was formed, however, the surface roughness increases again after 100 cycles LBL growth, with the film having a thickness of 104.8 ± 11.7 nm (Fig. 10).

The XRD patterns of HKUST-1 thin films grown by the LBL method until 80 cycles show only two reflections at $2\theta = 11.6^{\circ}$ and 17.5°, which can be indexed to the (222) and (333) planes of HKUST-1, respectively, and the intensity of these peaks increases with increasing LBL cycles (Fig. 9G). However, new diffraction peaks appear after 100 cycles at $2\theta = 6.7^{\circ}$, 9.5°, and 13.6°, which can be indexed to the (200), (220), and (400) planes of the HKUST-1, respectively, implying less favorable, non-oriented growth starting with adsorption of reactive precursors from the solution. This result is presumably correlated with increases the surface roughness again after 100 cycles LBL growth (Fig. 10). We therefore conclude that ~80 cycles LBL growth of HKUST-1 generating ~90 nm of thickness under the conditions used in this study is required for realization of a high quality uniform film with oriented growth on thermal SiO_2 surfaces.

4. Conclusions

Thermal SiO_2 surfaces without thiol-based organic SAM layers were directly used to produce highly oriented HKUST-1 thin films along the [111] direction. XPS analysis supports the conclusion that

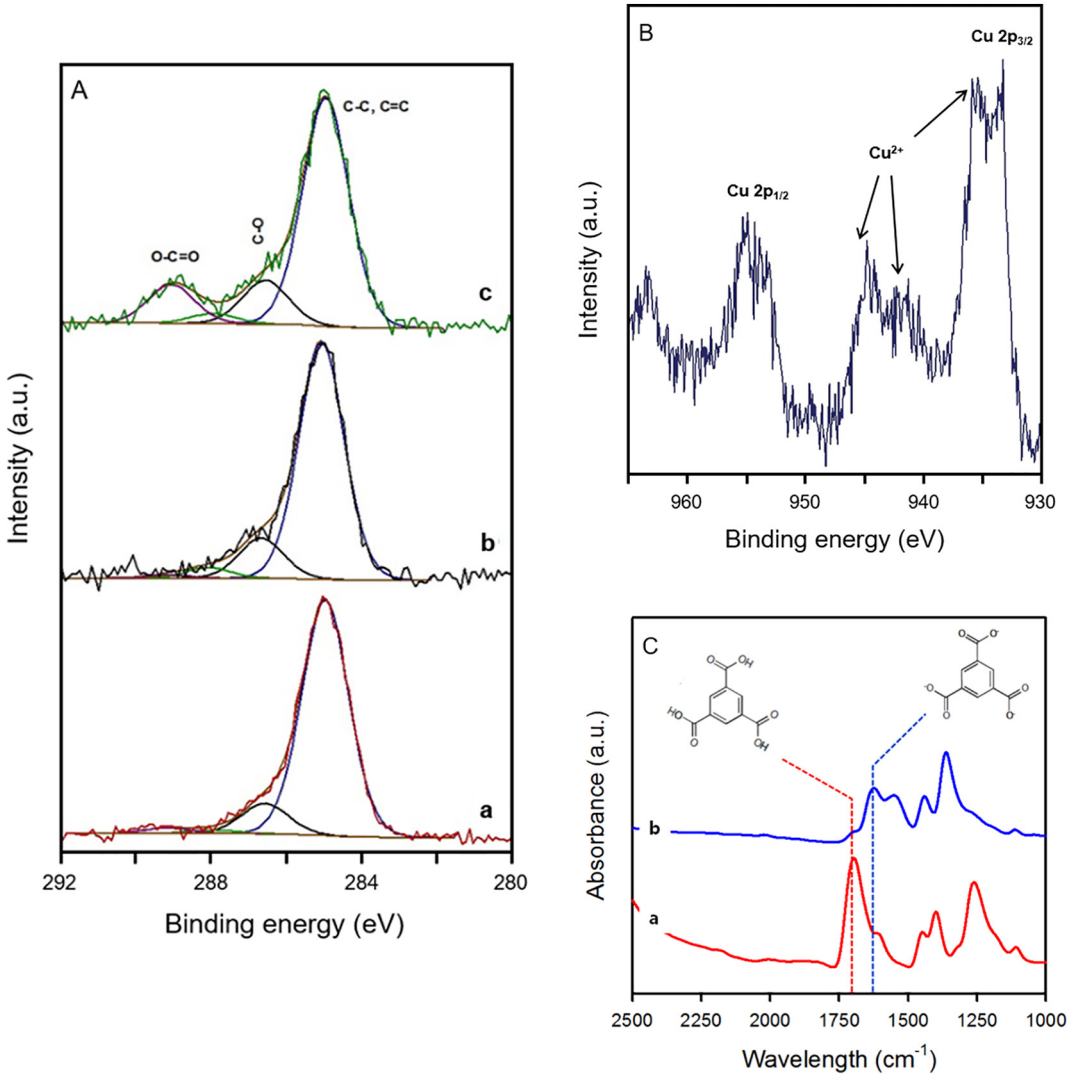

Fig. 6. XPS spectra in the (A) C 1 s (a: bare thermal SiO_2, b: after immersion into H_3BTC solution, c: after immersion into $Cu(OAc)_2$ solution) and (B) Cu 2p after immersion into $Cu(OAc)_2$ solution. (C) FT-IR spectra of (a) BTC and (b) HKUST-1 showing that a deprotonation reaction occurred in the synthesis of HKUST-1 from BTC.

the deposition of HKUST-1 by LBL growth on the thermal SiO_2 surface is initiated by deposition of $Cu(OAc)_2$ on the surface, followed by ligand exchange of coordinated acetate from the copper precursor with BTC ligands, eventually leading to crystallite coalescence to form a dense film. TEM analysis indicates that the growth species first form individual nanoparticles on thermal SiO_2 surfaces as seed sites, which then grow with increasing LBL cycles. The thicknesses of the HKUST-1 films can be readily controlled by the number of LBL growth cycles, and uniform surface coverage with highly oriented growth was obtained at ~80 cycles of LBL growth under the conditions used in this study. We believe that a better understanding of nucleation and growth of highly oriented MOF thin films on an oxide surface is a fundamental step in the preparation of optoelectronic devices such as chemical sensors, and provides important information in the development and study of MOF-based thin films with new and unique properties.

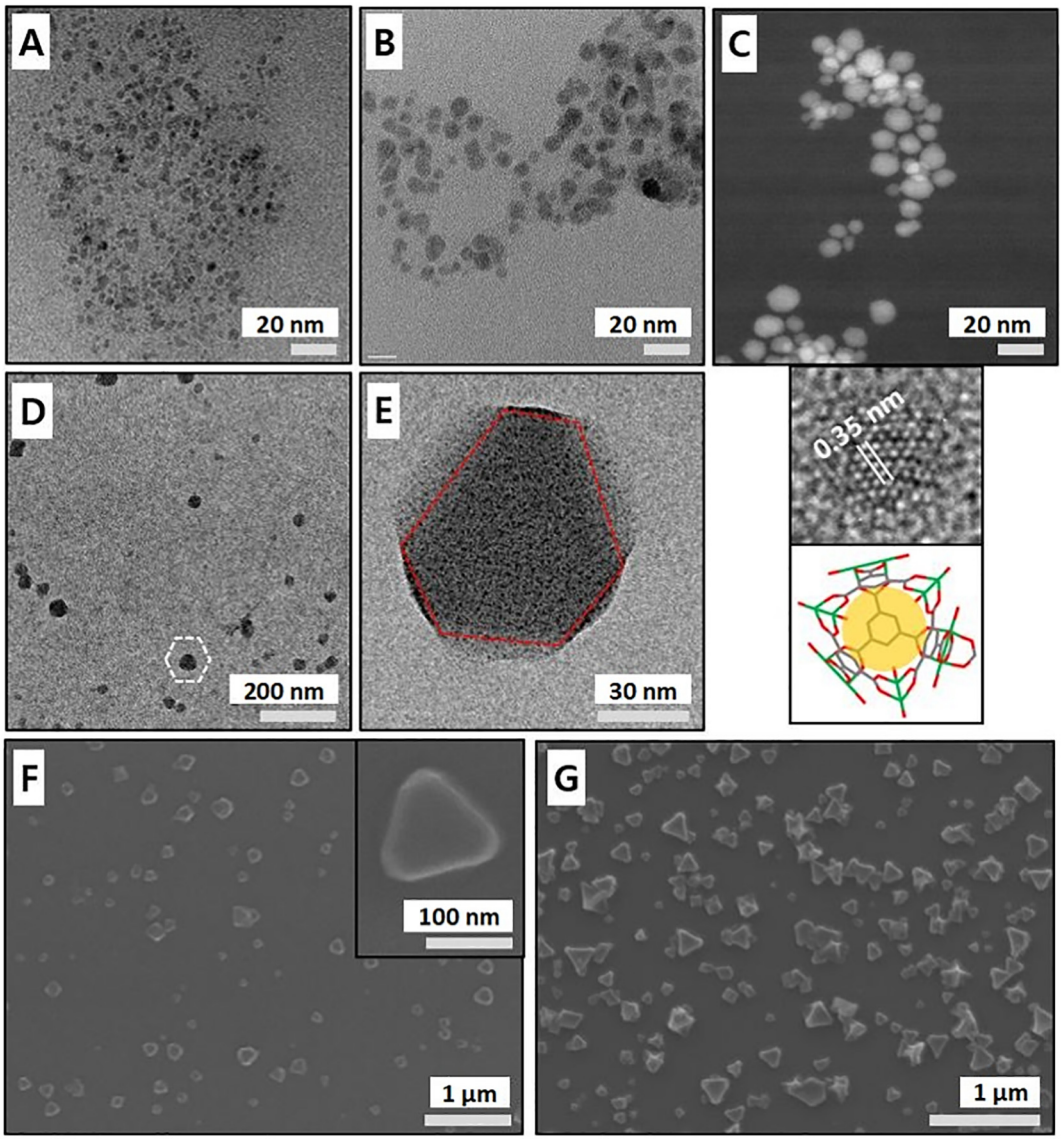

Fig. 7. Representative (A-E) TEM (or STEM) and (F, G) SEM images of the HKUST-1 LBL growth on thermal SiO_2 surface. (A) 2 cycles (2.7 nm average diameter), (B) 4 cycles (4.5 nm average diameter), (C) 6 cycles (8.3 nm average diameter, insert of HRTEM image and corresponded crystal structure of HKUST-1 showing the tetrahedral side pockets with triangular windows of 0.35 nm in diameter which are open to main channels. Red = oxygen, green = copper, and gray = carbon.), (D) 8 cycles (25.2 nm average diameter), (E) Magnified image from particles indicated by dotted hexagonal line in Fig. 4D, (F) 10 cycles (92.7 nm average diameter), and (G) 15 cycles. Corresponding SEM image of single particles (insets to F).

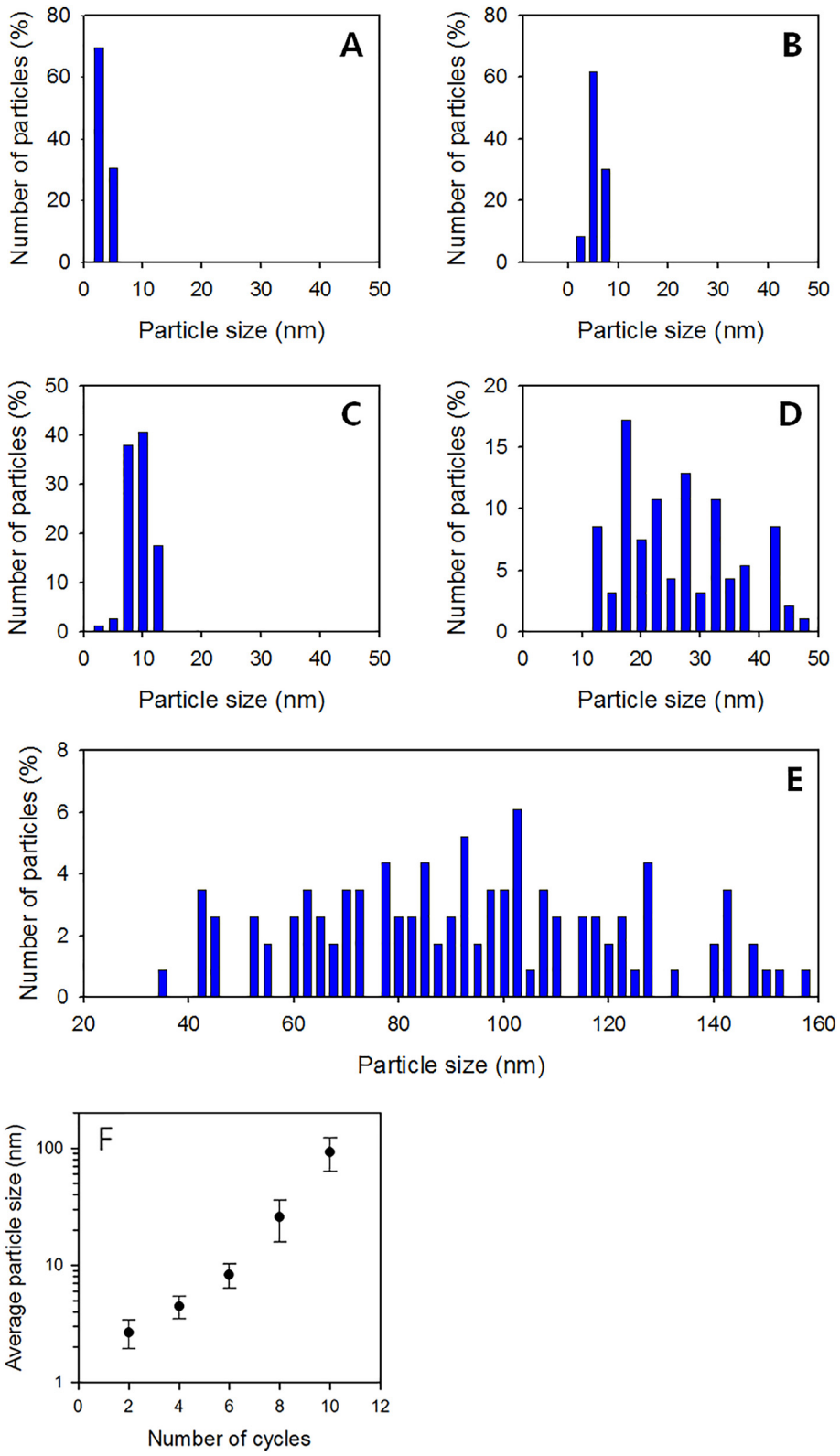

Fig. 8. Histograms of the particles grown on commercial SiO_2 support film by (A) 2 cycles, (B) 4 cycles, (C) 6 cycles, (D) 8 cycles, and (E) 10 cycles. (F) Average particle size grown on commercial SiO_2 support film versus numbers of LBL growth cycles. This size difference can be mainly attributed to the different nucleation kinetics and growth kinetics on the thermal SiO_2 surface.

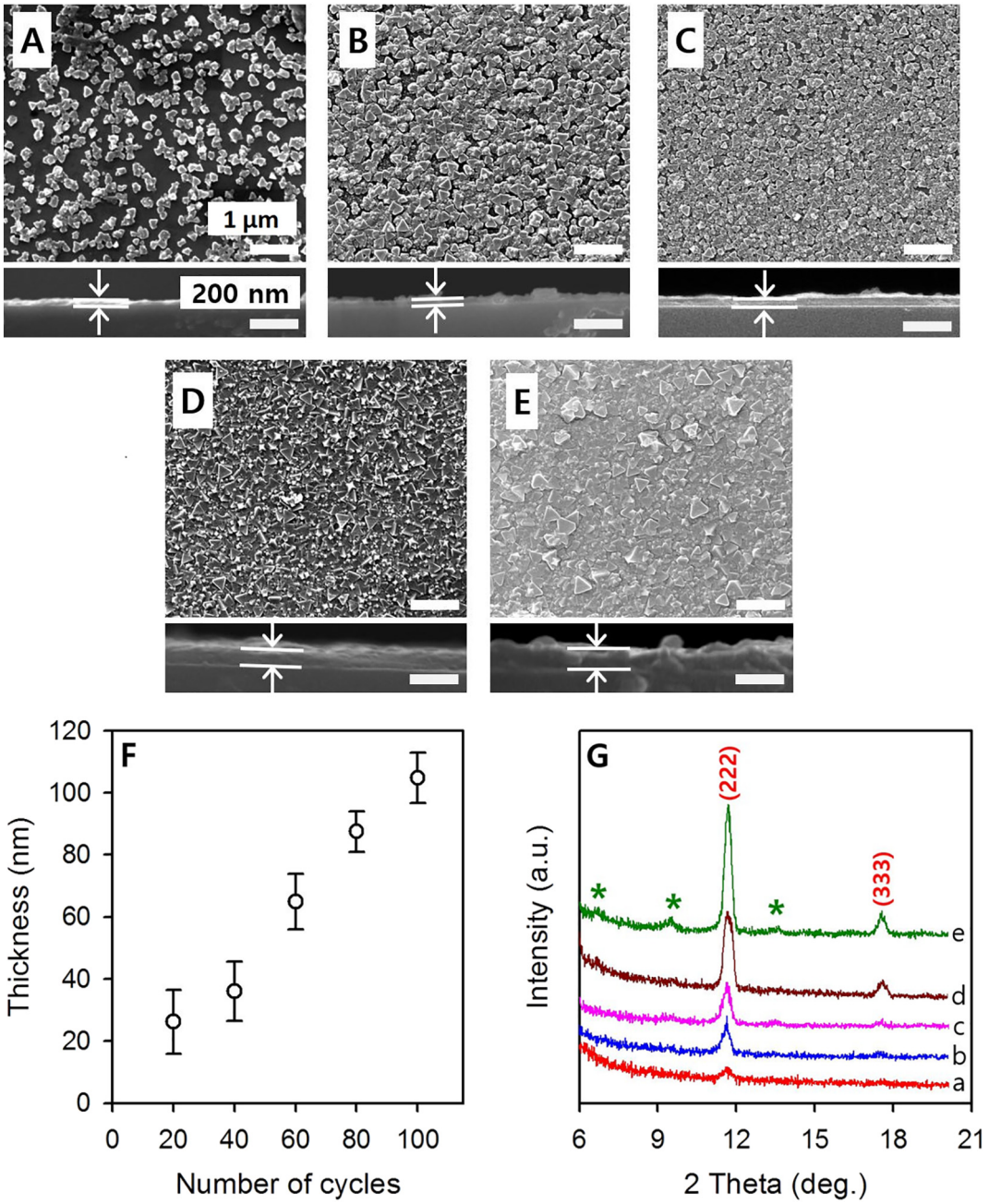

Fig. 9. Top and cross-sectional SEM images of the HKUST-1 grown on thermal 107 nm-SiO_2 surface of the (A) 20 cycles, (B) 40 cycles, (C) 60 cycles, (D) 80 cycles, and (E) 100 cycles LBL growth. (F) Thickness of HKUST-1 films versus numbers of LBL growth cycles. The error bars are derived from measurements of film roughness obtained by AFM. (G) XRD patterns of the HKUST-1 thin films grown on thermal 107 nm-SiO_2 surface. The peaks indicated by the asterisks, left to right, are the (200), (220), and (400) planes, respectively (a: 20 cycles, b: 40 cycles, c: 60 cycles, d: 80 cycles, and e: 100 cycles LBL growth).

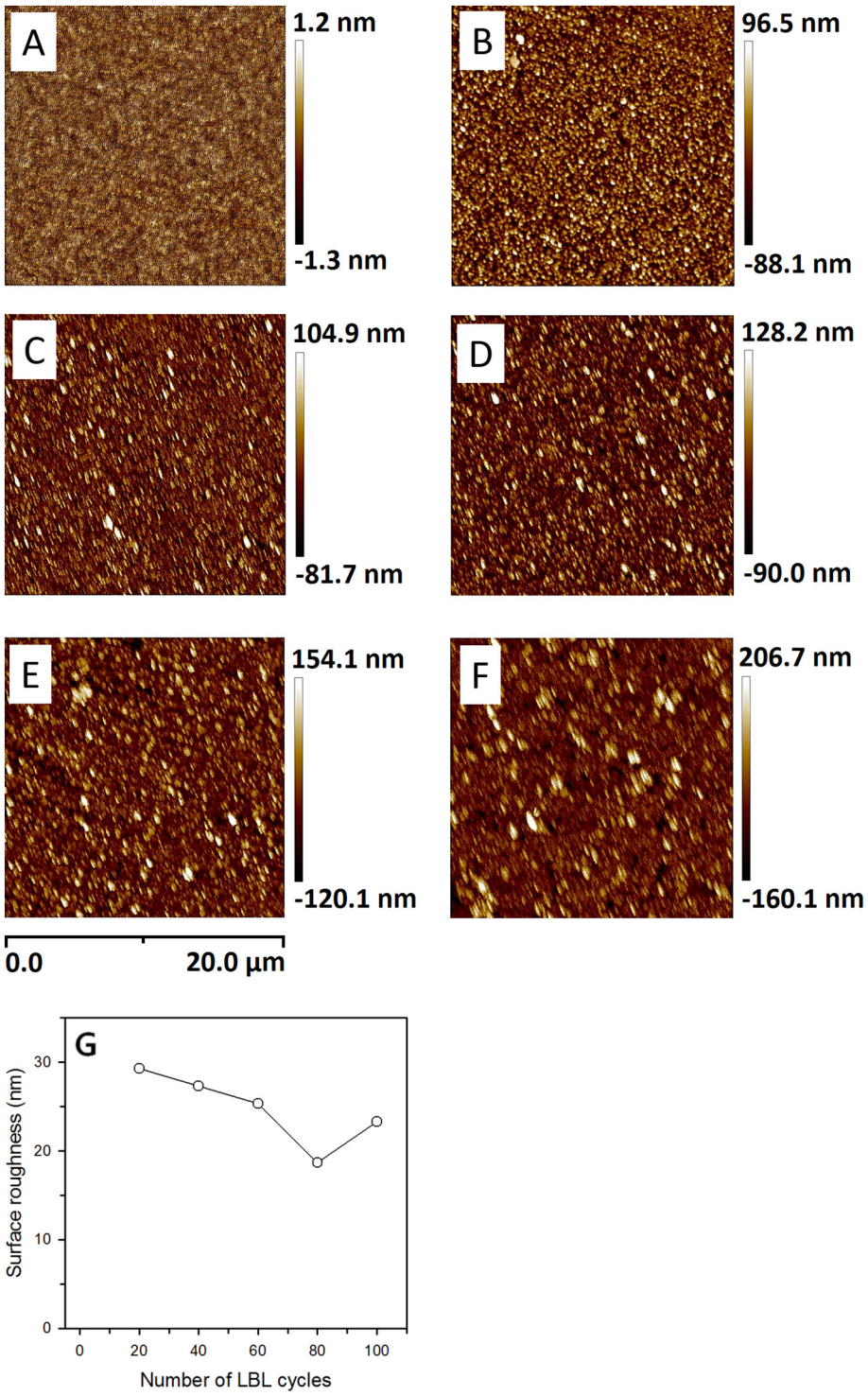

Fig. 10. AFM images of the HKUST-1 thin films after different number of LBL growth cycles on thermal SiO_2 surface. (A) 0 cycle, (B) 20 cycles, (C) 40 cycles, (D) 60 cycles, (E) 80 cycles, and (F) 100 cycles. (G) Surface roughness confirmed by AFM of HKUST-1 films versus numbers of LBL growth cycles.

Acknowledgements

This technical effort was performed in support of the National Energy Technology Laboratory's ongoing research under the RES contract DE-FE0004000. This project was also partially funded by the National Science Foundation under grant No. 1707506 and Scalable Nanomanufacturing Program under Grant No. CBET-1449383. Part of this work was conducted at the Oregon Process Innovation Center, a National Nanotechnology Coordinated Infrastructure site at the Oregon State University which is supported in part by the National Science Foundation (grant ECC-1542101) and Oregon State University. The TEM is funded by the National Science Foundation via the Major Research Instrumentation (MRI) Program under Grant No. 1040588. We would like to thank Teresa Sawyer and Zhongwei Gao, for experimental assistance. Neither the United States Government nor any agency thereof, nor any of their employees, makes any warranty, expressed or implied, or assumes any legal liability or responsibility for the accuracy, completeness, or usefulness of any information,

apparatus, product, or process disclosed, or represents that its use would not infringe privately owned rights. Reference herein to any specific commercial product, process, or service by trade name, trademark, manufacturer, or otherwise, does not necessarily constitute or imply its endorsement, recommendation, or favoring by the United States Government or any agency thereof. The views and opinions of authors expressed herein do not necessarily state or reflect those of the United States Government or any agency thereof.

References

[1] D. Zacher, O. Shekhah, C. Wöll, R.A. Fischer, Thin films of metal-organic frameworks, Chem. Soc. Rev. 38 (2009) 1418–1429.
[2] O. Shekhah, J. Liu, R. Fischer, C. Wöll, MOF thin films: existing and future applications, Chem. Soc. Rev. 40 (2011) 1081–1106.
[3] D. Bradshaw, A. Garai, J. Huo, Metal-organic framework growth at functional interfaces: thin films and composites for diverse applications, Chem. Soc. Rev. 41 (2012) 2344–2381.
[4] A. Bétard, R.A. Fischer, Metal-organic framework thin films: from fundamentals to applications, Chem. Rev. 112 (2011) 1055–1083.
[5] H. Gliemann, C. Wöll, Epitaxially grown metal-organic frameworks, Mater. Today 15 (2012) 110–116.
[6] M.W. Terban, D. Banerjee, S. Ghose, B. Medasani, A. Shukla, B.A. Legg, Y. Zhou, M.L. Sushko, J.J. De Yoreo, J. Liu, P. Thallapally, S.J.L. Billinge, Early stage structural development of prototypical zeolitic imidazolate framework (ZIF) in solution, Nanoscale 10 (2018) 4291–4300.
[7] J. Liu, B. Lukose, O. Shekhah, H.K. Arslan, P. Weidler, H. Gliemann, S. Bräse, S. Grosjean, A. Godt, X. Feng, A novel series of isoreticular metal organic frameworks: realizing metastable structures by liquid phase epitaxy, Sci. Rep. 2 (2012) 921.
[8] M. Tu, R.A. Fischer, Heteroepitaxial growth of surface mounted metal-organic framework thin films with hybrid adsorption functionality, J. Mater. Chem. A 2 (2014) 2018–2022.
[9] Z. Wang, J. Liu, B. Lukose, Z. Gu, P.G. Weidler, H. Gliemann, T. Heine, C. Wöll, Nanoporous designer solids with huge lattice constant gradients: multiheteroepitaxy of metal-organic frameworks, Nano Lett. 14 (2014) 1526–1529.
[10] V. Chernikova, O. Shekhah, M. Eddaoudi, Advanced fabrication method for the preparation of MOF thin films: liquid-phase epitaxy approach meets spin coating method, ACS Appl. Mater. Interfaces 8 (2016) 20459–20464.
[11] O. Shekhah, M. Eddaoudi, The liquid phase epitaxy method for the construction of oriented ZIF-8 thin films with controlled growth on functionalized surfaces, Chem. Commun. 49 (2013) 10079–10081.
[12] O. Shekhah, L. Fu, R. Sougrat, Y. Belmabkhout, A.J. Cairns, E.P. Giannelis, M. Eddaoudi, Successful implementation of the stepwise layer-by-layer growth of MOF thin films on confined surfaces: mesoporous silica foam as a first case study, Chem. Commun. 48 (2012) 11434–11436.
[13] O. Shekhah, H. Wang, T. Strunskus, P. Cyganik, D. Zacher, R. Fischer, C. Wöll, Layer-by-layer growth of oriented metal organic polymers on a functionalized organic surface, Langmuir 23 (2007) 7440–7442.
[14] O. Shekhah, H. Wang, S. Kowarik, F. Schreiber, M. Paulus, M. Tolan, C. Sternemann, F. Evers, D. Zacher, R.A. Fischer, Step-by-step route for the synthesis of metal-organic frameworks, J. Am. Chem. Soc. 129 (2007) 15118–15119.
[15] O. Shekhah, H. Wang, D. Zacher, R.A. Fischer, C. Wöll, Growth mechanism of metal-organic frameworks: insights into the nucleation by employing a step-by-step route, Angew. Chem. Int. Ed. 48 (2009) 5038–5041.
[16] O. Shekhah, Layer-by-layer method for the synthesis and growth of surface mounted metal-organic frameworks (SURMOFs), Dent. Mater. 3 (2010) 1302–1315.
[17] O. Zybaylo, O. Shekhah, H. Wang, M. Tafipolsky, R. Schmid, D. Johannsmann, C. Wöll, A novel method to measure diffusion coefficients in porous metal-organic frameworks, Phys. Chem. Chem. Phys. 12 (2010) 8093–8098.
[18] D. Zacher, K. Yusenko, A. Bétard, S. Henke, M. Molon, T. Ladnorg, O. Shekhah, B. Schüpbach, T. de los Arcos, M. Krasnopolski, Liquid-phase epitaxy of multicomponent layer-based porous coordination polymer thin films of [M(L)(P)0.5] type: importance of deposition sequence on the oriented growth, Chem. Eur. J. 17 (2011) 1448–1455.
[19] H.K. Arslan, O. Shekhah, J. Wohlgemuth, M. Franzreb, R.A. Fischer, C. Wöll, High-throughput fabrication of uniform and homogenous MOF coatings, Adv. Funct. Mater. 21 (2011) 4228–4231.
[20] M. Hanke, H.K. Arslan, S. Bauer, O. Zybaylo, C. Christophis, H. Gliemann, A. Rosenhahn, C. Wöll, The biocompatibility of metal-organic framework coatings: an investigation on the stability of SURMOFs with regard to water and selected cell culture media, Langmuir 28 (2012) 6877–6884.
[21] J. Liu, O. Shekhah, X. Stammer, H.K. Arslan, B. Liu, B. Schüpbach, A. Terfort, C. Wöll, Deposition of metal-organic frameworks by liquid-phase epitaxy: the influence of substrate functional group density on film orientation, Dent. Mater. 5 (2012) 1581–1592.
[22] V. Stavila, J. Volponi, A.M. Katzenmeyer, M.C. Dixon, M.D. Allendorf, Kinetics and mechanism of metal-organic framework thin film growth: systematic investigation of HKUST-1 deposition on QCM electrodes, Chem. Sci. 3 (2012) 1531–1540.
[23] T. Ladnorg, A. Welle, S. Heißler, C. Wöll, H. Gliemann, Site-selective growth of surface-anchored metal-organic frameworks on self-assembled monolayer patterns prepared by AFM nanografting, Beilstein J. Nanotechnol. 4 (2013) 638.
[24] L. Heinke, C. Wöll, Adsorption and diffusion in thin films of nanoporous metal-organic frameworks: ferrocene in SURMOF $Cu_2(ndc)_2(dabco)$, Phys. Chem. Chem. Phys. 15 (2013) 9295–9299.
[25] V. Stavila, A.A. Talin, M. Allendorf, MOF-based electronic and opto-electronic devices, Chem. Soc. Rev. 43 (2014) 5994–6010.
[26] S.J. Dalgarno, P.K. Thallapally, L.J. Barbour, J.L. Atwood, Engineering void space in organic van der Waals crystals: calixarenes lead the way, Chem. Soc. Rev. 36 (2007) 236–245.
[27] G. Lu, O.K. Farha, L.E. Kreno, P.M. Schoenecker, K.S. Walton, R.P. Van Duyne, J.T. Hupp, Fabrication of metal-organic framework-containing silica-colloidal crystals for vapor sensing, Adv. Mater. 23 (2011) 4449–4452.
[28] K.-J. Kim, Y.J. Li, P.B. Kreider, C.-H. Chang, N. Wannenmacher, P.K. Thallapally, H.-G. Ahn, High-rate synthesis of Cu-BTC metal-organic frameworks, Chem. Commun. 49 (2013) 11518–11520.
[29] P. Swift, Adventitious carbon-the panacea for energy referencing? Surf. Interface Anal. 4 (1982) 47–51.
[30] D.B. Mawhinney, J.A. Glass, J.T. Yates, FTIR study of the oxidation of porous silicon, J. Phys. Chem. B 101 (1997) 1202–1206.
[31] R. Tian, O. Seitz, M. Li, W. Hu, Y.J. Chabal, J. Gao, Infrared characterization of interfacial Si-O bond formation on silanized flat SiO_2/Si surfaces, Langmuir 26 (2010) 4563–4566.
[32] K.T. Queeney, N. Herbots, J.M. Shaw, V. Atluri, Y. Chabal, Infrared spectroscopic analysis of an ordered Si/SiO_2 interface, J, Appl. Phys. Lett. 84 (2004) 493–495.
[33] X.-H. Guan, G.-H. Chen, C. Shang, ATR-FTIR and XPS study on the structure of complexes formed upon the adsorption of simple organic acids on aluminum hydroxide, J. Environ. Sci. 19 (2007) 438–443.
[34] C.-A. Tao, J. Wang, S. Qin, Y. Lv, Y. Long, H. Zhu, Z. Jiang, Fabrication of pH-sensitive graphene oxide-drug supramolecular hydrogels as controlled release systems, J. Mater. Chem. 22 (2012) 24856–24861.
[35] D. Payer, A. Comisso, A. Dmitriev, C. Woll, A. DeVita, J.V. Barth, K. Kern, Ionic hydrogen bonds controlling two-dimensional supramolecular systems at a metal surface, Chem. Eur. J. 13 (2007) 3900–3906.
[36] M.A. Brookshier, C.C. Chusuei, D.W. Goodman, Control of CuO particle size on SiO_2 by spin coating, Langmuir 15 (1999) 2043–2046.
[37] C.C. Chusuei, M.A. Brookshier, D.W. Goodman, Correlation of relative X-ray photoelectron spectroscopy shake-up intensity with CuO particle size, Langmuir 15 (1999) 2806–2808.
[38] E.S. Shpiro, W. Grünert, R.W. Joyner, G.N. Baeva, Nature, distribution and reactivity of copper species in over-exchanged Cu-ZSM-5 catalysts: an XPS/XAES study, Catal. Lett. 24 (1994) 159–169.
[39] J.P. Espinós, J. Morales, A. Barranco, A. Caballero, J.P. Holgado, A.R. González-Elipe, Interface effects for Cu, CuO, and Cu_2O deposited on SiO_2 and ZrO_2. XPS determination of the valence state of copper in Cu/SiO_2 and Cu/ZrO_2 catalysts, J. Phys. Chem. B 106 (2002) 6921–6929.
[40] L. Peng, J. Zhang, J. Li, B. Han, Z. Xue, G. Yang, Surfactant-directed assembly of mesoporous metal-organic framework nanoplates in ionic liquids, Chem. Commun. 48 (2012) 8688–8690.
[41] S.S.-Y. Chui, S.M.-F. Lo, J.P.H. Charmant, A.G. Orpen, I.D. Williams, A chemically functionalizable nanoporous material $[Cu_3(TMA)_2(H_2O)_3]$n, Science 283 (1999) 1148–1150.
[42] E. Biemmi, C. Scherb, T. Bein, Oriented growth of the metal organic framework $Cu_3(BTC)_2(H_2O)_3{\cdot}xH_2O$ tunable with functionalized self-assembled monolayers, J. Am. Chem. Soc. 129 (2007) 8054–8055.
[43] D. Zacher, A. Baunemann, S. Hermes, R.A. Fischer, Deposition of microcrystalline $[Cu_3(btc)_2]$ and $[Zn_2(bdc)_2(dabco)]$ at alumina and silica surfaces modified with patterned self-assembled organic monolayers: evidence of surface selective and oriented growth, J. Mater. Chem. 17 (2007) 2785–2792.
[44] J.-L. Zhuang, D. Ceglarek, S. Pethuraj, A. Terfort, Rapid room-temperature synthesis of metal-organic framework HKUST-1 crystals in bulk and as oriented and patterned thin films, Adv. Funct. Mater. 21 (2011) 1442–1447.
[45] R.E. Morris, How does your MOF grow? ChemPhysChem 10 (2009) 327–329.
[46] N.S. John, C. Scherb, M. Shoaee, M.W. Anderson, M.P. Attfield, T. Bein, Single layer growth of sub-micron metal-organic framework crystals observed by in situ atomic force microscopy, Chem. Commun. 45 (2009) 6294–6296.